Mean flow and turbulence measurements in a triangular turbulent free jet

W. R. Quinn
Department of Engineering, St. Francis Xavier University, Antigonish, Nova Scotia, Canada

Detailed mean flow and turbulence measurements were made, using hot-wire anemometry, in the near flow field of a turbulent, incompressible air jet issuing from a sharp-edged equilateral triangular slot into stagnant air surroundings. The measured quantities included the three components of the mean velocity vector, the three turbulence intensities, and two of the Reynolds shear stresses. The results indicate that the jet spreads faster on its base side than at its apex. This difference in spreading leads to an inversion of the jet shape at about five equivalent slot diameters downstream from the slot exit plane. The Reynolds shear stress levels, compared to those found in round turbulent free jets at the same downstream locations, are higher in the triangular jet, implying improved mixing.

Keywords: triangular jet; turbulence; sharp-edged slot

Introduction

Triangular turbulent free jets, like other turbulent free jets issuing from noncircular slots or nozzles, are used or have the potential for use in technical areas of interest ranging from aerospace to chemical to mechanical engineering. Some areas of application of triangular turbulent jets are in combustion chambers of jet engines, boiler furnaces, and gas-turbine plants of electric power utilities. Rapid mixing is a prerequisite for good performance in most applications. Economic expediency may, in some applications, require that sharp-edged slots be used in preference to nozzles with contoured upstream shaping.

Previous experimental work on triangular turbulent free jets[1-3] has involved jets issuing from either isosceles and equilateral triangular ducts[1] or from isosceles and equilateral triangular orifices,[2,3] with small upstream bell-mouth radii, attached to pipes of circular cross section. These flow configurations occur, along with sharp-edged slots, in practical systems. The flow of a turbulent free jet, issuing from a sharp-edged triangular slot has thus far, however, not been studied.

This study presents detailed mean flow and turbulence data for the flow, in the near flow field, of a turbulent, incompressible air jet issuing from a sharp-edged equilateral triangular slot into stagnant air surroundings. The decay of the mean streamwise velocity along the jet centerline is also presented. The slot exit plane Reynolds number, based on the equivalent diameter of the triangular slot (same as the diameter of a round slot with the same exit area as the triangular slot), was about 2.08×10^5. The mean streamwise velocity and streamwise turbulence intensity at the center of the slot exit plane were $60\,m\,s^{-1}$ and 0.5%, respectively.

Experimental arrangement and procedure

The flow facility, described in detail elsewhere,[4] is of the blow-down type and consists of a small centrifugal fan, a settling chamber, a three-dimensional (3-D) contraction and the sharp-edged equilateral triangular slot. The equilateral triangular slot was assembled, in a machined retaining plate, from three machine-mitered pieces of aluminum. One of the aluminum pieces is shown by solid lines in Figure 1; the other two pieces are shown by dashed lines. The fan draws air from a room adjacent to the laboratory and feeds it to the settling chamber, which is fitted with a baffle at its upstream end, an aluminum honeycomb with hexagonal cells and five mesh-wire screens of 69% porosity. The 3-D contraction, which is attached to the downstream end of the settling chamber, has a contour that is based on a third-degree polynomial with zero derivative end conditions. The sharp-edged equilateral triangular slot caps the downstream end of the 3-D contraction. The jet issues from the slot into a cage, which is open at the downstream end and covered on the top and sides with steel damping screens of 42% porosity.

The sensing probe is moved in the flow field by a stepping-motor-driven, microcomputer-controlled, 3-D traversing system. Positioning accuracy is 0.3 mm in the streamwise (x) direction and 0.01 mm in the spanwise (y) and lateral (z) directions. A definition sketch of the coordinate system and the corresponding components of the mean velocity vector is presented in Figure 2. A rack-and-pinion system is used for traversing in the x direction, and lead screws are used for traversing in the y and z directions.

X-array hot-wire probes were used for the mean flow and turbulence measurements. The hot-wire probes, operated by linearized constant temperature anemometers at a resistance ratio of 1.8, were calibrated in the initial region of the test jet. The two wires of the X-array probes were matched by yawing the probes slightly (by about 0.5°). Corrections for temperature variations from the calibration temperature and for the effect of tangential cooling were made in the data reduction software. A 12-bit A/D board, with 16 analog input channels, a multiplexer, and a sample-and-hold unit, was used to digitize the hot-wire signals. Signal conditioning was effected by two other sample-and-hold units, low-pass analog filters with a 5-kHz cut-off frequency and 40-dB/decade roll-off and amplifiers. The mean and rms fluctuating velocities were obtained by sampling between 75,000 and 100,000 points at 1 kHz, depending on the location in the flow.

Address reprint requests to Dr. Quinn at the Department of Engineering, St. Francis Xavier University, Antigonish, Nova Scotia, Canada B2G 1C0.

Received 10 July 1989; accepted 12 February 1990

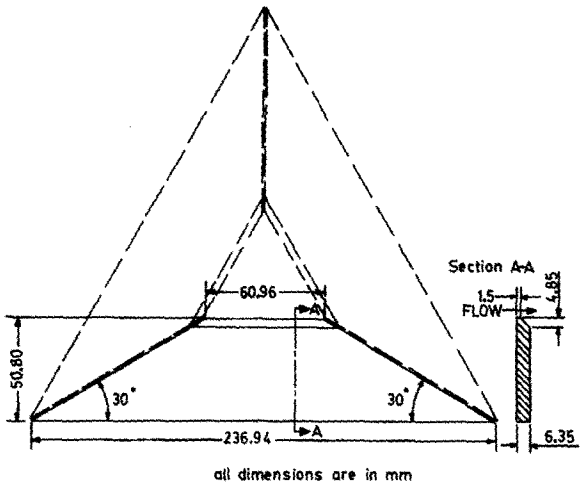

Figure 1 Sharp-edged equilateral triangular slot detail

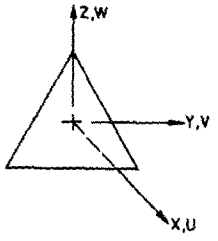

Figure 2 Definition sketch for the coordinate system

Results and discussion

Mean velocity

The decay of the mean streamwise velocity along the jet centerline is shown in Figure 3(a). The results for jets issuing from a sharp-edged round slot and from a contoured round nozzle with the same exit area as that of the triangular slot are included for comparison. These results were obtained in the same test rig used for the triangular jet. The vena contracta effect, associated with sharp-edged slots,[5] is clearly evident in the jets issuing from the sharp-edged slots. The maximum value of U_{Cl}/U_{exit} for the triangular jet in Figure 3(a) is 1.44. By contrast, the jet issuing from the contoured round nozzle does not have the exit mean streamwise velocity overshoot found in the other two jets. The inverse decay plots for the three jets and that for the round jet investigated by Wygnanski and Fiedler[6] are shown in Figure 3(b). The jets issuing from the sharp-edged slots have higher mean streamwise velocity decay rates than those issuing from the contoured nozzles. Higher mean streamwise velocity decay rates imply better far-field

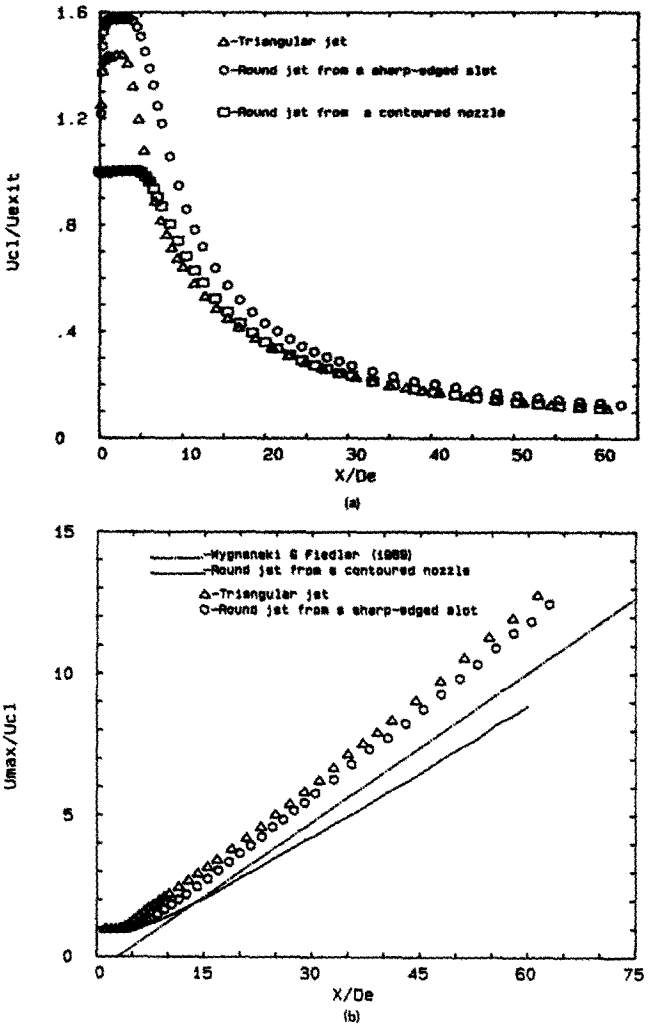

Figure 3 (a) Mean streamwise velocity decay along the jet centerline; (b) inverse decay plots

Notation

D_e	Equivalent slot diameter
U	Mean streamwise velocity
$\sqrt{\overline{u'^2}}$	Root mean square of the fluctuating streamwise velocity
$\overline{-u'v'}$	Reynolds shear stress in the x–y plane
$\overline{-u'w'}$	Reynolds shear stress in the x–z plane
V	Mean spanwise velocity
$\sqrt{\overline{v'^2}}$	Root mean square of the fluctuating spanwise velocity
$\overline{v'^2}$	Reynolds normal stress in the y direction
$\overline{-v'w'}$	Reynolds shear stress in the y–z plane
W	Mean lateral velocity
$\sqrt{\overline{w'^2}}$	Root mean square of the fluctuating lateral velocity
$\overline{w'^2}$	Reynolds normal stress in the z direction
x	Streamwise cartesian coordinate
y	Spanwise cartesian coordinate
z	Lateral cartesian coordinate
∇^2	Laplacian operator

Greek symbols

ν	Kinematic viscosity of fluid
Ω_x	Mean streamwise vorticity
Ω_y	Mean spanwise vorticity
Ω_z	Mean lateral vorticity

Subscripts

Cl	Centerline value
exit	Value at the center of the slot exit plane
max	Maximum value on the jet centerline

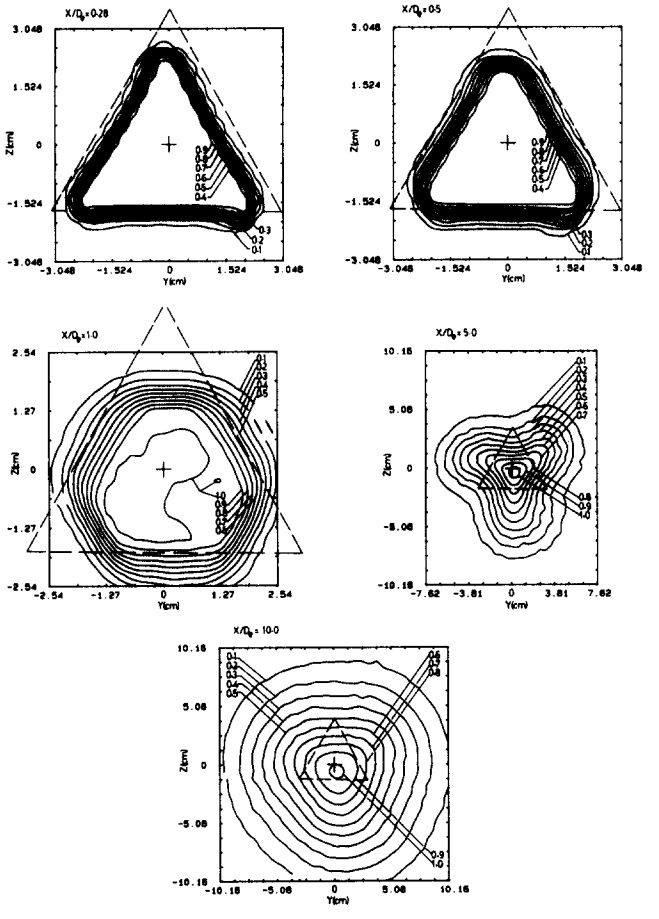

Figure 4 U/U_{CI} contours

mixing. The potential core lengths of the sharp-edged triangular and round slot jets, deduced from Figure 3(b), are $3.1D_e$ and $4.4D_e$, respectively. The shorter potential core length of the triangular jet, also evident in Figure 3(a) and in agreement with the results of Gutmark *et al.*,[1] indicates better near-field mixing.

Mean streamwise velocity contours plots at five downstream stations are presented in Figure 4. In the region close to the slot exit plane ($x/D_e=0.28$ and $x/D_e=0.5$), the contours have the triangular shape prescribed by the slot. Furthermore, the 0.5 contour is farther from the center of the jet—shown by a cross in Figure 4 and in all subsequent figures—on the apex side than on the base side of the jet. This difference indicates faster spreading of the jet on its apex side in this region of the flow. At $x/D_e=1$, the contours have a quasi-axisymmetric shape, and spreading on the base side is now faster than on the apex side. Farther downstream (at $x/D_e=5$ and at $x/D_e=10$), the contours have an inverted triangular shape, but faster spreading still occurs on the base side of the jet as viewed from the slot exit plane. The changing shape of the mean streamwise velocity field of the jet as it develops downstream, in view of the subsequent discussion in connection with the Reynolds stresses, is noteworthy. The difference in the size of the triangular slot—superimposed with dashed lines on all the figures showing contour maps—is caused by the contour-plotting software, which enlarges the measurement grid for $x/D_e \leqq 1$ and contracts it for $x/D_e > 1$.

Contours of the mean spanwise velocity and the mean lateral velocity are shown in Figure 5(a) and (b), respectively. The secondary flow pattern, in the near-flow field, is made up of four counterrotating cells. The spanwise secondary flow cells suggest inflow at the base side and outflow at the apex side of the jet. The lateral secondary flow cells suggest flow from the apex side into the base side of the jet. The combined effect of the spanwise and lateral secondary flow cells is consistent with the faster spreading of the jet on its base side, as noted earlier.

Turbulence quantities

The streamwise turbulence intensity variation along the jet centerline is shown in Figure 6. The results for jets issuing from a sharp-edged round slot and from a contoured round nozzle are included for comparison. A steep increase in the streamwise turbulence intensity is observed in all three flows initially. This increase is a consequence of shear layer growth and the resulting high production of turbulence, which is then diffused from the shear layers to the jet centerline. The higher streamwise turbulence intensity values in the triangular jet flow, in the initial region, provide further evidence of better near-field mixing in the triangular jet. The decrease in the streamwise turbulence intensity in the triangular jet flow, in the region $x/D_e=8$–10, reflects the drop in turbulent activity that accompanies the merging of the shear layers emanating from the three sides of the equilateral triangular slot.

The streamwise turbulence intensity contours are presented in Figure 7. The shapes of the mean streamwise velocity contours, presented in Figure 4, and those of the streamwise turbulence intensity contours at the corresponding downstream

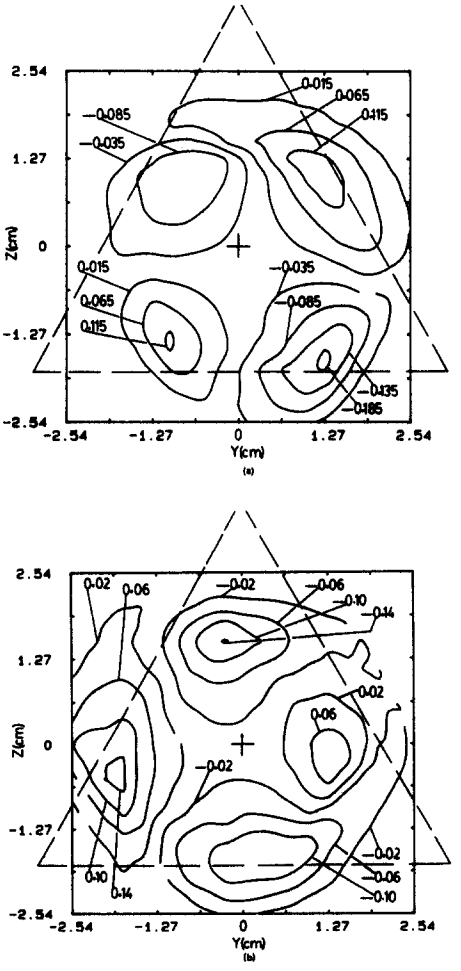

Figure 5 (a) V/U_{CI} contours at $x/D_e=1.0$; (b) W/U_{CI} contours at $x/D_e=1.0$

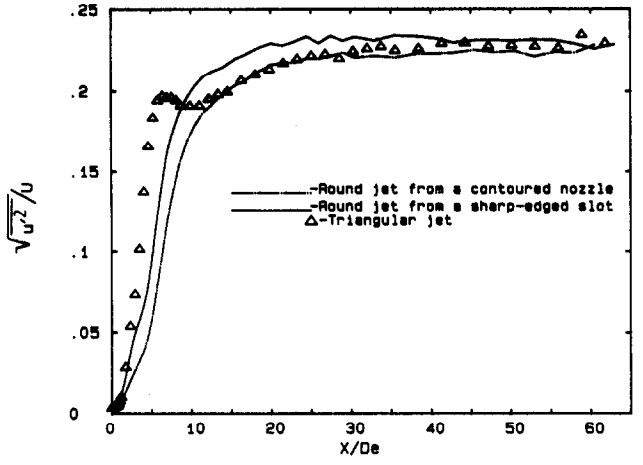

Figure 6 Streamwise turbulence intensity variation along the jet centerline

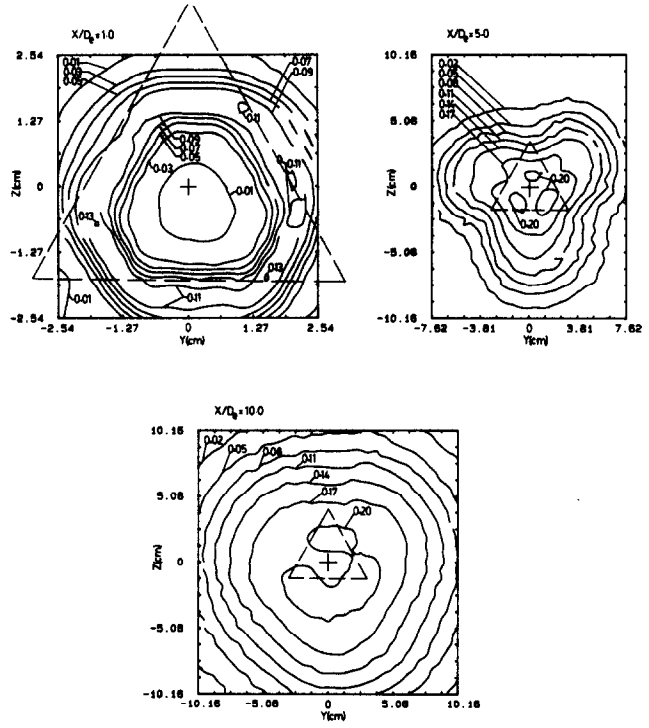

Figure 7 $\sqrt{\overline{u'^2}}/U_{CI}$ contours

stations in Figure 7 correspond closely. Furthermore, large streamwise turbulence intensity gradients are found, as expected,[7] in regions where the local shear in the mean streamwise velocity is high and vice versa. The spanwise and lateral turbulence intensity contours are shown in Figures 8 and 9, respectively. The shapes of the spanwise and lateral turbulence intensity contours are similar to those of the streamwise turbulence intensity contours. However, the maximum values of the spanwise and lateral turbulence intensities are less than those of the streamwise turbulence intensities at all the downstream stations. These results reflect the fact that the spanwise and lateral velocity fluctuations acquire their energy, by means of pressure fluctuations, from the streamwise velocity fluctuations. The Reynolds normal stresses, derivable from the turbulence intensities by squaring, are clearly anisotropic. Such anisotropy of the spanwise and lateral Reynolds normal stresses triggers turbulence-generated secondary flows[8] (Prandtl's secondary flows of the second kind), which represent streamwise vorticity production. The transport of the mean streamwise vorticity in a steady, incompressible flow is given by

$$U\frac{\partial\Omega_x}{\partial x}+V\frac{\partial\Omega_x}{\partial y}+W\frac{\partial\Omega_x}{\partial z}=\Omega_x\frac{\partial U}{\partial x}+\Omega_y\frac{\partial U}{\partial y}+\Omega_z\frac{\partial U}{\partial z}$$
$$+\left(\frac{\partial^2}{\partial z^2}-\frac{\partial^2}{\partial y^2}\right)(\overline{v'w'})+\frac{\partial^2}{\partial y\,\partial z}(\overline{v'^2}-\overline{w'^2})$$
$$+\frac{\partial}{\partial x}\left(\frac{\partial\overline{u'v'}}{\partial z}-\frac{\partial\overline{u'w'}}{\partial y}\right)+\nu\nabla^2\Omega_x \qquad (1)$$

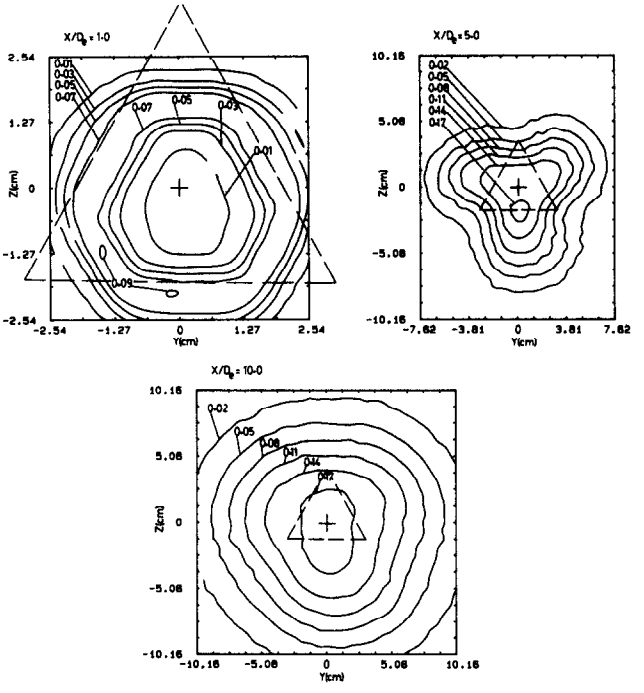

Figure 8 $\sqrt{\overline{v'^2}}/U_{CI}$ contours

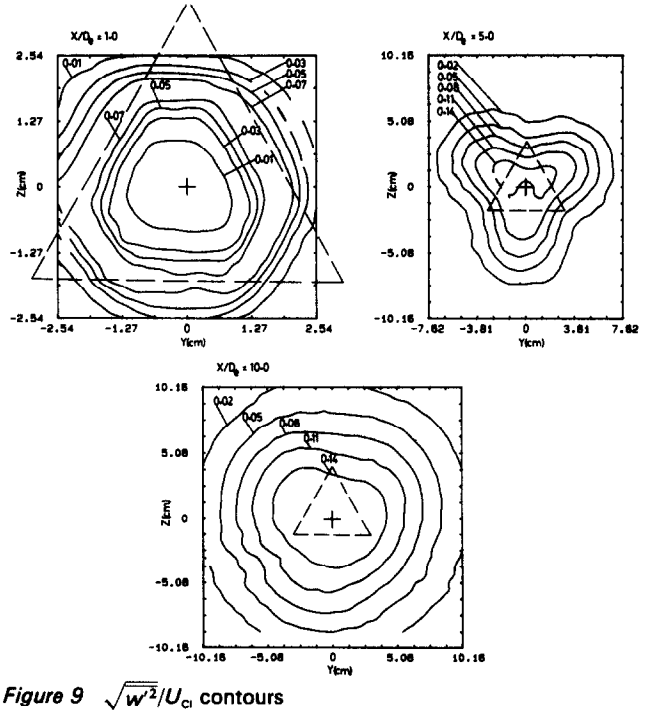

Figure 9 $\sqrt{\overline{w'^2}}/U_{CI}$ contours

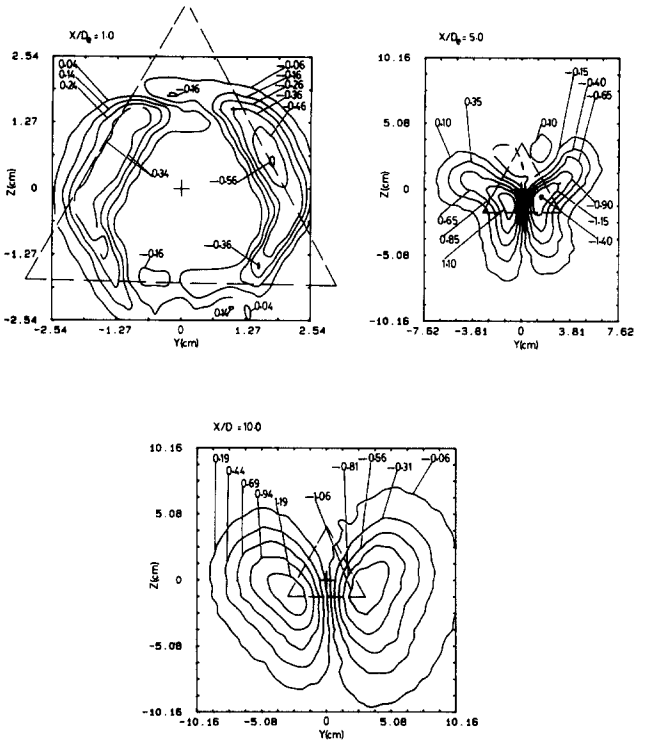

Figure 10 $(-\overline{u'v'}/U_{CL}^2 \times 100)$ contours

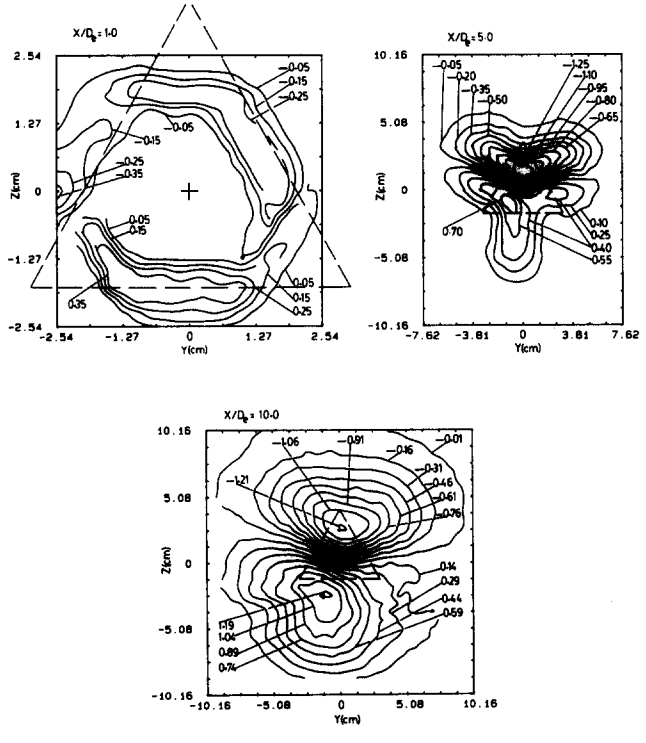

Figure 11 $(-\overline{u'w'}/U_{CL}^2 \times 100)$ contours

The fourth, fifth, and sixth terms on the right-hand side of Equation 1 represent secondary flows of Prandtl's second kind. The sixth term is usually negligibly small, as a result of the boundary layer approximation, compared to the other two,[8] which are responsible for the change in shape of the mean streamwise velocity field with downstream distance,[9] as noted earlier.

The Reynolds shear stress contours are shown in Figures 10 and 11. Like the streamwise turbulence intensity, large Reynolds shear stress gradients are also found in regions of the flow where the local shear in the mean streamwise velocity is large. The maximum Reynolds shear stress levels are generally larger than those found in round turbulent free jets at the corresponding downstream stations,[10,11] implying improved mixing. The $-\overline{v'w'}$ Reynolds shear stress was not measured. The difficulties and resulting large errors associated with the measurement of this component of the Reynolds stress tensor are well known.[8,9]

Conclusions

The mean flow and some turbulence characteristics in the near-field of an incompressible, turbulent free air jet, issuing from a sharp-edged equilateral triangular slot, were examined in detail. We found that the jet spreads faster at its base side than at its apex side. The faster base-side spreading leads to an inversion of the shape of the jet at about five equivalent slot diameters downstream from the slot exit plane. The maximum Reynolds shear levels in the triangular jet are higher than those in round turbulent free jets at the corresponding downstream locations, indicating improved mixing.

Acknowledgments

The support of the Natural Sciences and Engineering Research Council of Canada, through grant A5484, is gratefully acknowledged.

References

1 Gutmark, E., Schadow, K. C., Parr, D. M., Harris, C. K., and Wilson, K. C. The mean and turbulent structure of noncircular jets. AIAA paper no. 85-0543, 1985

2 Koshigoe, S., Gutmark, E., and Schadow, K. C. Wave structures in jets of arbitrary shape. III. Triangular jets. *Phys. Fluids*, 1988, **31**, 1410–1419

3 Schadow, K. C., Gutmark, E., Parr, D. M., and Wilson, K. C. Selective control of flow coherence in triangular jets. *Exp. Fluids*, 1988, **6**, 129–135

4 Quinn, W. R. and Militzer, J. Effects of nonparallel exit flow on round turbulent free jets. *Int. J. Heat and Fluid Flow*, 1989, **10**, 139–145

5 Daugherty, R. L., Franzini, J. B., and Finnemore, E. J. *Fluid Mechanics with Engineering Applications*, McGraw-Hill, New York, 1985

6 Wygnanski, I. and Fiedler, H. Some measurements in the self-preserving jet. *J. Fluid Mech.*, 1969, **38**, 577–612

7 Bradshaw, P. *An Introduction to Turbulence and its Measurement*, Pergamon, Oxford, England, 1975

8 Perkins, H. J. The formation of streamwise vorticity in turbulent flow. *J. Fluid Mech.*, 1970, **44**, 721–740

9 Bradshaw, P. Turbulent secondary flows. *Ann. Rev. Fluid Mech.*, 1987, **19**, 53–74

10 Sami, S., Carmody, T., and Rouse, H. Jet diffusion in the region of flow establishment. *J. Fluid Mech.*, 1967, **27**, 231–252

11 Boguslawski, L. and Popiel, Cz. O. Flow structure of the free round turbulent jet in the initial region. *J. Fluid Mech.*, 1979, **90**, 531–539